Meteorol Atmos Phys (2018) 130:427–440
https://doi.org/10.1007/s00703-017-0528-7

ORIGINAL PAPER

Spatio-temporal evolution characteristics and prediction of dry–wet abrupt alternation during the summer monsoon in the middle and lower reaches of the Yangtze River Basin

Lijie Shan[1,3] · Liping Zhang[1,2] · Zhe Xiong[4] · Xinchi Chen[1,3] · Shaodan Chen[1,3] · Wei Yang[1,3]

Received: 25 September 2016 / Accepted: 2 May 2017 / Published online: 9 May 2017
© Springer-Verlag Wien 2017

Abstract Summer rainfall anomalies have often posed a major water concern in China, and the variations and prediction of dry–wet abrupt alternation (DWAA) events have been receiving increasing attention from researchers. Based on precipitation and atmospheric circulation indices in the middle and lower reaches of the Yangtze River Basin, the spatio-temporal evolution characteristics and predictability of DWAA events were analyzed by calculating the dry–wet abrupt alternation index and selecting early warning signals. The results indicate that most long-cycle and short-cycle DWAA events, except in the period of May–June, are wet-to-dry (WTD) events and that the frequencies and intensities of WTD events have gradually decreased over time. The spatial distribution characteristics on the south shore of the Yangtze River are opposite to those on the north shore. Occurrences of DWAA events can be predicted to some extent by comparing the actual and critical values of select early warning signals. The results also indicate that the BP neural network model exhibits strong performance in simulating the occurrences of DWAA events and therefore may provide a useful reference for intraseasonal wet and dry management in the Yangtze River Basin.

Responsible Editor: A. P. Dimri.

✉ Liping Zhang
zhanglp@whu.edu.cn

[1] State Key Laboratory of Water Resources and Hydropower Engineering Science, Wuhan University, Wuhan 430072, China

[2] College of Tourism Culture and Geographical Science, Huanggang Normal University, Huanggang 438000, China

[3] Hubei Collaborative Innovation Center for Water Resources Security, Wuhan 430072, China

[4] Key Lab of Regional Climate-Environment for East Asia (TEA), Institute of Atmospheric Physics, Chinese Academy of Sciences, Beijing 100029, China

1 Introduction

Widespread increases in global temperatures may influence the probability and the intensity of extreme precipitation events (Schaer et al. 1996; Groisman et al. 1999), resulting in phenomena such as an abrupt wet spell after a prolonged dry spell, which can be defined as a dry–wet abrupt alternation (DWAA) event. These extreme fluctuations between dry spells and wet spells may seriously impact human systems, agricultural yields and infrastructure (Turner and Annamalai 2012).

The middle and lower reaches of the Yangtze River Basin (YRB-ML) (106°54′–124°25′E, 24°30′–35°45′N) are located in a typical monsoon climate region with a drainage area of 800,000 km^2 (Fig.1). The annual precipitation in the basin is approximately 1300 mm, with a decreasing trend from the southeast to the northwest. The basin also features an obviously nonuniform annual distribution of precipitation, as more than 60% of the annual precipitation falls between May and August every year. The climate of the area is influenced by two types of monsoon per year, the southeast Asian summer monsoon (May–September) and the northwest Siberian winter monsoon (October–April) (Tao and Ding 1981; Su et al. 2006). It is humid and rainy during the summer monsoon and became cold and dry during the winter monsoon. The anomalous activities of the summer monsoon will bring droughts and flood disasters, and severe temperature decreases, snowfall events and gales may occur under the activity of the winter

monsoon in the area (Tao and Ding 1981; Zhang and Wang 1997). Rainfall is concentrated and rainfall anomalies occur most frequently during the summer season, mainly because precipitation is closely associated with a quasi-stationary front (or mei-yu belt), which represents the activity of the summer monsoon (Ho et al. 2003). Therefore, understanding the temporal and spatial evolution characteristics of DWAA events and their predictability during summertime in YRB-ML is crucial for preventing disasters and managing water resources.

Summer rainfall anomalies have been discussed in a number of studies (Kruger 1999; Reason et al. 2005; Weaver et al. 2009; Efstathiou and Varotsos 2012; Chaudhuri and Pal 2014; Muhire et al. 2015). In particular, intraseasonal rainfall anomalies have been receiving increasing attention since the 1990s (Camberlin 1997; Maheras et al. 1999; Gonzalez et al. 2008; Chikoore and Jury 2010; Kim et al. 2014; Yao et al. 2014). DWAA events, a typical form of intraseasonal precipitation anomaly, have occurred more frequently in various regions of China in recent years (Wu et al. 2006; Zhang et al. 2007; Sun et al. 2012). Wu et al. (2006) quantified the summer intraseasonal long-cycle droughts–floods abrupt alternation (LDFA) phenomenon by defining an LDFA index and analyzed its correlation with large-scale atmospheric circulation anomalies. Cheng et al. (2012) identified DWAA events by combining Standardized Precipitation Index (SPI) and historical disaster data, and summarized their spatio-temporal evolution characteristics and corresponding circulation features in the Huai River Basin. Furthermore, Li and Ye (2015) selected the DWAA events in the Poyang Lake Basin, and analyzed their temporal, and spatial distribution characteristics and tendencies. Most studies have focused on the evolutionary characteristics of DWAA events, with little attention paid to the simulation or prediction of these events.

The objective of this study is to analyze the spatial and temporal characteristics of DWAA from three aspects in YRB-ML during the summer monsoon period (1960–2012, from May to August), and simulate and predict the occurrences of these events using the methods of stepwise regression and back propagation neural network modeling.

2 Data and methods

2.1 Data

The daily precipitation data sets for 75 meteorological stations distributed evenly all over the study basin for the period of 1960–2012 were obtained from the National Meteorological Information Center of China. Moreover, 74 atmospheric circulation indices published by the National Climate Center were obtained. In addition, the atmospheric circulation fields for the Southern Hemisphere Annular Mode Index (SAMI), the Northern Hemisphere Annular Mode Index (NAMI) and the North Atlantic Oscillation Index (NAOI) for the same period were available from the Institute of Atmospheric Physics, Chinese Academy of Sciences. These indices were used as predictive factors for predicting the occurrence of DWAA events.

2.2 Methods

2.2.1 Identification of DWAA event

For each station and the overall study area, standardized precipitation anomalies (SPA) (Maheras et al. 1999) have been calculated as follows:

$$\mathrm{SPA}_i = \frac{P_i - \overline{P}}{\sigma}, \tag{1}$$

where P_i is the precipitation of a particular month, i represents the month, $\overline{P}$ and σ are the long-term monthly mean and standard deviation, respectively. Months with standardized precipitation anomalies that are less than -0.5 or greater than 0.5 standard deviations are defined as dry spells and wet spells, respectively.

To describe the DWAA phenomena quantitatively and qualitatively, a dry–wet abrupt alternation index (DWAAI) was defined by Wu et al. (2006) and Zhang et al. (2012) as follows:

$$\mathrm{DWAAI} = (\mathrm{SPA}_i - \mathrm{SPA}_{i-1}) \cdot (|\mathrm{SPA}_i| + |\mathrm{SPA}_{i-1}|) \cdot \alpha^{-|\mathrm{SPA}_i + \mathrm{SPA}_{i-1}|} \quad (i = 1, 2, \ldots n), \tag{2}$$

where SPA_{i-1} and SPA_i refer to the standardized precipitation anomalies in the $i-1$ month and the i month, respectively, $(\mathrm{SPA}_i - \mathrm{SPA}_{i-1})$ represents the DWAA intensity term, $(|\mathrm{SPA}_i| + |\mathrm{SPA}_{i-1}|)$ represents the intensity of the wet and dry, and $\alpha^{-|\mathrm{SPA}_i + \mathrm{SPA}_{i-1}|}$ is the weighting coefficient, which enhances the weights of DWAA events and reduces the weights of persistent wet and dry phenomena.

In this paper, the spatio-temporal evolution characteristics of DWAA were grouped into both long-cycle and short-cycle time scales. Long-cycle time scale was defined as 2 months, i.e., 2 months of wet conditions and 2 months of dry conditions, based on the hydro-meteorological characteristics of the basin. Therefore, long-cycle DWAA events correspond to wet (dry) throughout May–June and dry (wet) throughout July–August. According to the study by Wu et al. (2006), the DWAAI calculated with $\alpha = 1.8$ was suitable for long-cycle DWAA events selection. Similarly, the short-cycle time scale was defined as 1 month,

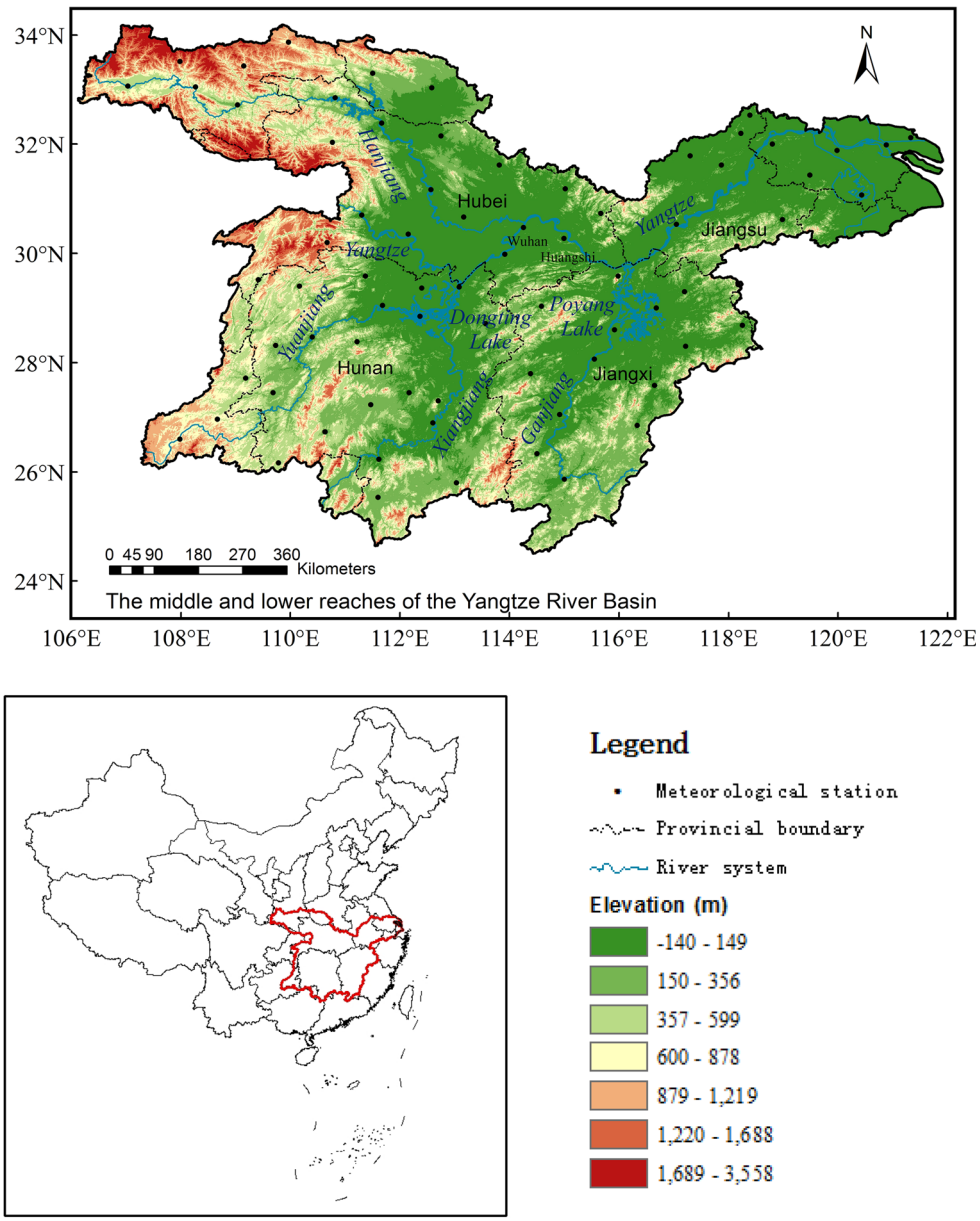

Fig. 1 Location of the middle and lower reaches of the Yangtze River Basin. The *black dots* denote the meteorological stations. Provincial boundaries (*black lines*) and first-order streams in the basin (in *blue*) are shown

and the α value of 3.2 was used to calculate the short-cycle DWAAI (Zhang et al. 2012). In addition, scenarios with DWAAI of less than −1 and greater than 1 were regarded as wet-to-dry (WTD) events and dry-to-wet (DTW) events, respectively. Moreover, a higher absolute DWAAI value indicates an incident of higher severity.

2.2.2 *Stepwise regression (SR)*

To understand the relationship between long-term atmospheric circulation and DWAA events and to predict the occurrence of such events, stepwise regression (SR) modeling was applied to pick out best combination of circulation indices for predicting the DWAAI of both long- and short-cycle time scales.

Stepwise regression is a combination of forward selection and backward elimination (Ghani and Ahmad 2010). In this method, variables are added to and removed from the model with the greatest influence on the residual sum of squares in each step (Bilgili 2010). In the forward selection procedure, the new subset model is chosen by adding one variable at a time to the previously chosen subset. The variable can be added to the subset model if it causes the residual sum of squares to decrease the most. The selection procedure changes to backward elimination if the residual sums of squares for any chosen variables do not meet a minimum criterion to stay. The backward process eliminates the variable whose deletion causes the least increase in the residual sum of squares until all chosen variables meet the minimum criterion. The selection process

terminates when no variables outside the model meet the criterion to enter and when all variables in the model meet the criterion to stay. Thus, the number of independent variables in the best combination is not guaranteed (Cevik 2007).

2.2.3 Back propagation (BP) neural network

Back propagation (BP) neural network is a multi-layer feed-forward network algorithm proposed by Rumelhart et al. (1986). Importantly, this algorithm provides a powerful mathematical or computational technique for modeling systems in which the relationship among the variables is unknown (Fausett 1994). In general, neural networks are regarded as non-linear input–output models and have been used in different research fields (French et al. 1992; Karunanithi et al. 1994; Shamseldin 1997; Ghorbani et al. 2016).

In this paper, a three-layer BP neural network, which contains only one hidden layer, was applied to simulate DWAAI and to predict the occurrence of DWAA events. The input information for the network consisted of the predictive factors selected via stepwise regression, and the output information was the DWAAI value. For neurons in the hidden and output layers, the input power Y_{net} was calculated with the following equation (Haykin 1994):

$$Y_{\text{net}} = \sum_{i=1}^{N} Y_i \omega_i + \omega_0, \tag{3}$$

where N is the number of neurons in the preceding layer; Y_i is the output of the ith neuron in the preceding layer; ω_i is the connection weight between the neuron and the ith neuron in the preceding layer; and ω_0 is the neuron threshold value. The neuron output Y_{out} is obtained from the neuron input Y_{net} through the following neuron transfer function:

$$Y_{\text{out}} = f(Y_{\text{net}}) = \frac{1}{1 + e^{-Y_{\text{net}}}}. \tag{4}$$

The selected transfer function has an S shape, and its value ranges between 0 and 1; because of these characteristics, the function can introduce non-linearity into the operation of the neural network, which enhances its ability to represent a natural process. The output Y_{out} of the output layer is the final network output array. The output error E of the network, i.e., the error in the information transmitted to the output layer, can be calculated as follows:

$$E = \sum_{i=1}^{m} \frac{1}{2}(X_i - Y_{\text{out}i})^2, \tag{5}$$

where m is the number of neurons in the output layer; X_i and $Y_{\text{out}i}$ are the desired output and calculated output, respectively, of the ith neuron in the output layer. The neural network will run until E is less than the expected error e. Then, it will enter the phase of the backward propagation of error signals. The primary purpose of the backward propagation of error is to estimate ω_i and ω_0 (Hammerstrom 1993). Generally speaking, the two processes alternate until E is less than e or the training time has reached a preset value.

3 Results

3.1 Temporal evolution characteristics of DWAA events

The long-cycle dry–wet abrupt alternation index (LDWAAI) based on the average precipitation of the area during the period of 1960–2012 was calculated, and the years with the six highest and six lowest LDWAAI values and the corresponding SPAs of May–June and July–August are listed in Table 1. The high-LDWAAI years exhibit more rainfall in July–August than May–June, which suggests that high-LDWAAI years correspond to increased precipitation from May to August and that the inverse also holds true. Specifically, the July–August SPA for five of the high-LDWAAI years are greater than 0.5, and for three of those years, the values are greater than 1, indicating that these years represent a significant increase in moisture level (a wet spell). While

Table 1 Comparison of SPA values for the six highest and six lowest LDWAAI during periods of 1960–2012

High LDWAAI				Low LDWAAI			
Year	LDWAAI	May–June SPA	July–August SPA	Year	LDWAAI	May–June SPA	July–August SPA
1969	1.11	0.24	2.13	1967	−9.02	1.49	−1.70
1980	0.70	0.77	2.09	1971	−5.24	1.05	−1.83
1996	0.67	0.67	1.84	1964	−5.15	1.06	−1.63
2008	0.62	−0.19	0.73	2011	−3.25	0.88	−0.97
2007	0.52	−0.65	0.18	1995	−3.25	1.95	−0.67
1991	0.35	−0.04	0.67	1973	−2.77	1.99	−0.55

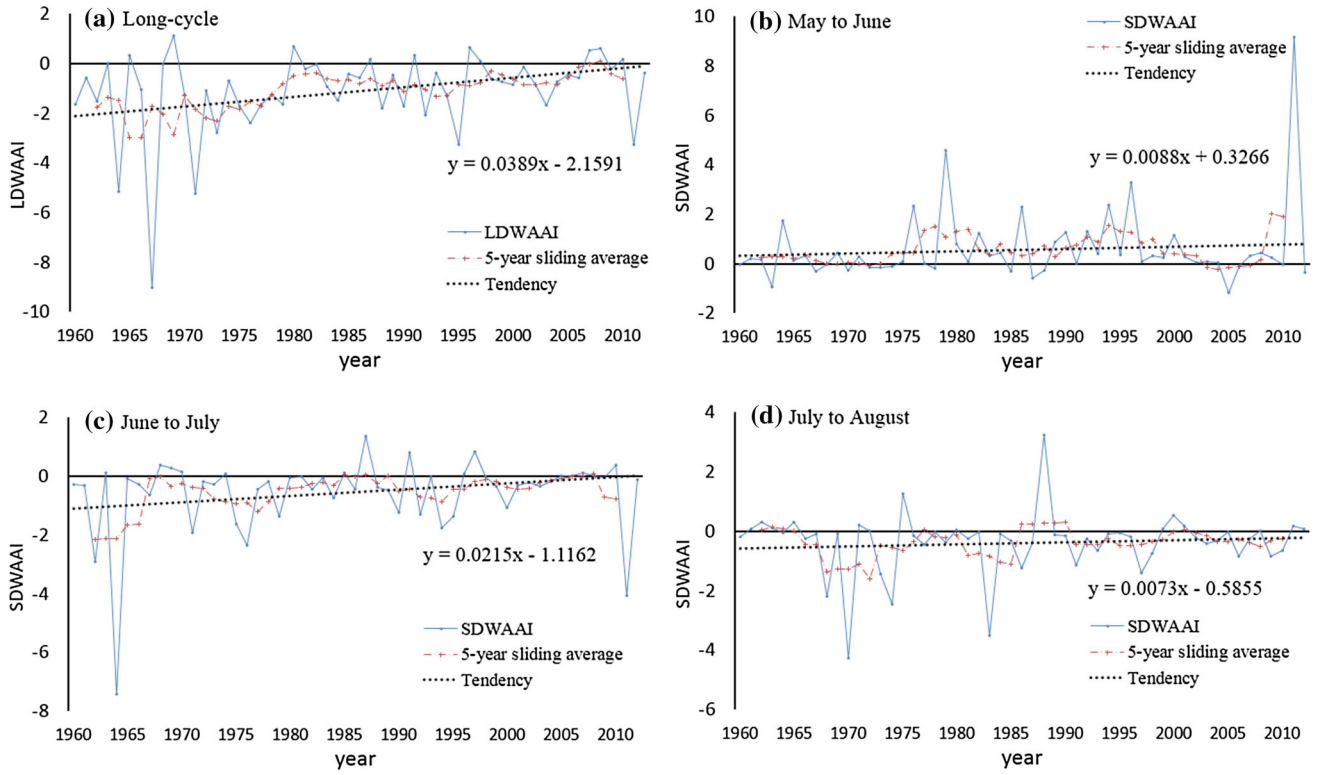

Fig. 2 The variation trends of **a** LDWAAI, SDWAAI during the periods of **b** May–June, **c** June–July and **d** July–August. The *blue lines* represent the calculated DWAAI. *Red dash lines* and *black dotted lines* represent the 5-year sliding average and tendency, respectively

Table 2 Statistical results for both WTD events and DTW events

Event type	Frequency	Years	Rate (%)
WTD	8	1964, 1967, 1971, 1973, 1976, 1988, 1995, 2011	15.10
DTW	1	1969	1.89

the May–June SPA of only one of these years is less than −0.5 (a dry spell). Therefore, high-LDWAAI values correctly reflect the occurrence of DTW events. The conditions of the low-LDWAAI years are precisely the opposite. The July–August SPAs of all chosen low-LDWAAI years are less than −0.5, even less than −1.0 in some years, but greater than 0.88 in May–June. Therefore, low-LDWAAI years are often related to WTD events.

The LDWAAI shows a significant increasing trend (10% significance level) since 1960 (Fig. 2a). It is clear that WTD events (LDWAAI <−1) are the main type of long-cycle dry–wet abrupt alternation (LDWAA) events. DWAA events can be identified by comparing the SPA in May–June with that in July–August (Table 2). There were three WTD events and one DTW (LDWAAI >1) event with high intensity in the 13-year period of 1960–1972, while only five WTD events in the 40-year period of 1973–2012. Therefore, LDWAA events have become less frequent since 1972. By also considering the 5-year sliding average, it is concluded that both the frequency and intensity of LDWAA events have gradually decreased over time.

The main type of short-cycle dry–wet abrupt alternation (SDWAA) event during the period of May–June is DTW and the corresponding short-cycle dry–wet abrupt alternation index (SDWAAI) fluctuated greatly during the period of 1975–1997 (Fig. 2b). Moreover, the 5-year sliding average curve shows that the frequency and intensity of DTW events during this period exhibit an increasing trend. In contrast, WTD is the main type during the period of June–July (Fig. 2c), and the SDWAAI fluctuated greatly during the period of 1960–1997. A tendency of transformation from WTD to DTW is evident, and a decrease in the incident intensity is observed. During the period of July–August (Fig. 2d), WTD is the main type of SDWAA event. The SDWAAI fluctuated greatly during the period of 1960–1997 and stabilized after 1990. In combination with the 5-year sliding average, these findings indicate that the frequency and intensity of SDWAA events during the period of July–August have gradually decreased over time.

DTW events occurred in certain areas during the study period, such as the western and northern regions of Hunan and the Jianghan Plain. For example, most of the area south of the Yangtze River was afflicted by a continuous dry spell prior to July 1988 largely as a result of continuous high-temperature climate, whereas continuing heavy rains occurred in the upper and middle reaches of the Yangtze River and Dongting Lake water system in mid-August. Notably, the precipitation has more than tripled compared to the same time last year. Moreover, the study area experienced the most severe continuous meteorological dry spell in the last six decades prior to June 2011, but then suffered from severe storm flooding disasters after four successive heavy precipitation events in June (Shen et al. 2012). The years in which severe disasters occurred coincided with those identified in this analysis as years with extreme DWAAI values, and these results demonstrate that the DWAAI can essentially reflect DWAA events.

3.2 Spatial distribution characteristics of DWAA events

3.2.1 Frequency

The spatial distribution of the frequency of DWAA events in study area is uneven (Fig. 3), i.e., DTW events tend to occur more commonly along the north shore of the Yangtze River, whereas WTD events tend to occur more commonly on the south shore. Figure 3a shows that the frequency of long-cycle WTD events on the south shore is higher, especially in the southeast. In contrast, long-cycle DTW events tend to occur on the north shore, especially in the northwest (Fig. 3b). This opposite feature is the result of the spatial variability in precipitation. On the south shore, annual maximum precipitation usually occurs in May and June, while it occurs in June and July on the north shore.

The spatial distributions of the frequency of WTD events in the three short-cycle periods, i.e., May–June, June–July and July–August, are nearly identical (Fig. 3c, e, g). There is a high incidence of WTD events on the south shore of the Yangtze River, and the frequencies in all periods are approximately the same. WTD events often occur in the middle area of the south shore during the period of May–June, whereas the high-incidence area shifts slightly eastward during the period of June–July, and it shifts to the west during the third period. Unlike WTD events, spatial distributions of the frequency of DTW events among these three periods are different (Fig. 3d, f, h). Specifically, YRB-ML is the high-incidence area of DTW events during the period of May–June. However, the northwestern parts and southern parts of the basin are the areas with the highest incidence of DTW events during the periods of June–July and July–August, respectively, but the frequency of such events is relatively lower.

3.2.2 Intensity

LDWAAI and SDWAAI calculated for each station in the typical years of 1998 and 2011 were used to analyze the spatial distributions of the intensity of DWAA events, as shown in Fig. 4. The spatial distributions of the intensity of LDWAA events in these two typical years were similar (Fig. 4a, b). Specifically, DTW events with high intensity occurred on the north shore of the Yangtze River. In contrast, WTD events predominantly occurred on the south shore, especially in 2011, when high-intensity WTD events occurred in most parts of the basin except in the northwestern region. In contrast, the LDWAA events in 1998 were more serious than those in 2011. Three stations experienced DTW events with SDWAAI values greater than 3.00 and five stations experienced high-intensity WTD events with SDWAAI values less than −5.00.

Intensity distributions of SDWAA events during the periods of May–June and June–July were roughly the same in both typical years, except more stations witnessed DWAA events in 2011 than in 1998 (Fig. 4c–f). Severe DTW events occurred in most parts of the basin from May to June and, by contrast, severe WTD events occurred at the same stations during the period of June–July. Unlike the LDWAA events, SDWAA events in 2011 were more serious than in 1998 during the two short-cycle periods. Severe WTD and DTW events were centered in the northwestern part during the periods of May–June and June–July, respectively. However, the intensity distributions of SDWAA events during the period of July–August were exactly opposite between 1998 and 2011 (Fig. 4g, h). Stations with a lower occurrence of DWAA events also observed lower intensities in these 2 years. Compared with LDWAAI, therefore, the SDWAAI can more accurately reflect the spatial distribution of the intensity of DWAA events.

3.2.3 Trends

The Mann–Kendall method (Mann 1945; Kendall 1975) was applied to analyze the spatial distributions of the trends of DWAA events and the results are presented in Fig. 5. This analysis suggests that considerable spatial differences exist in the trends of DWAA events in different stations.

LDWAAI exhibits an increasing trend in most of the study area except in the northwestern part, and an especially significant increasing trend is present in the Dongting Lake watershed (Fig. 5a). Therefore, the intensity of long-cycle WTD events is increasing in the northwestern part, but decreasing in the remainder of the basin. It should be

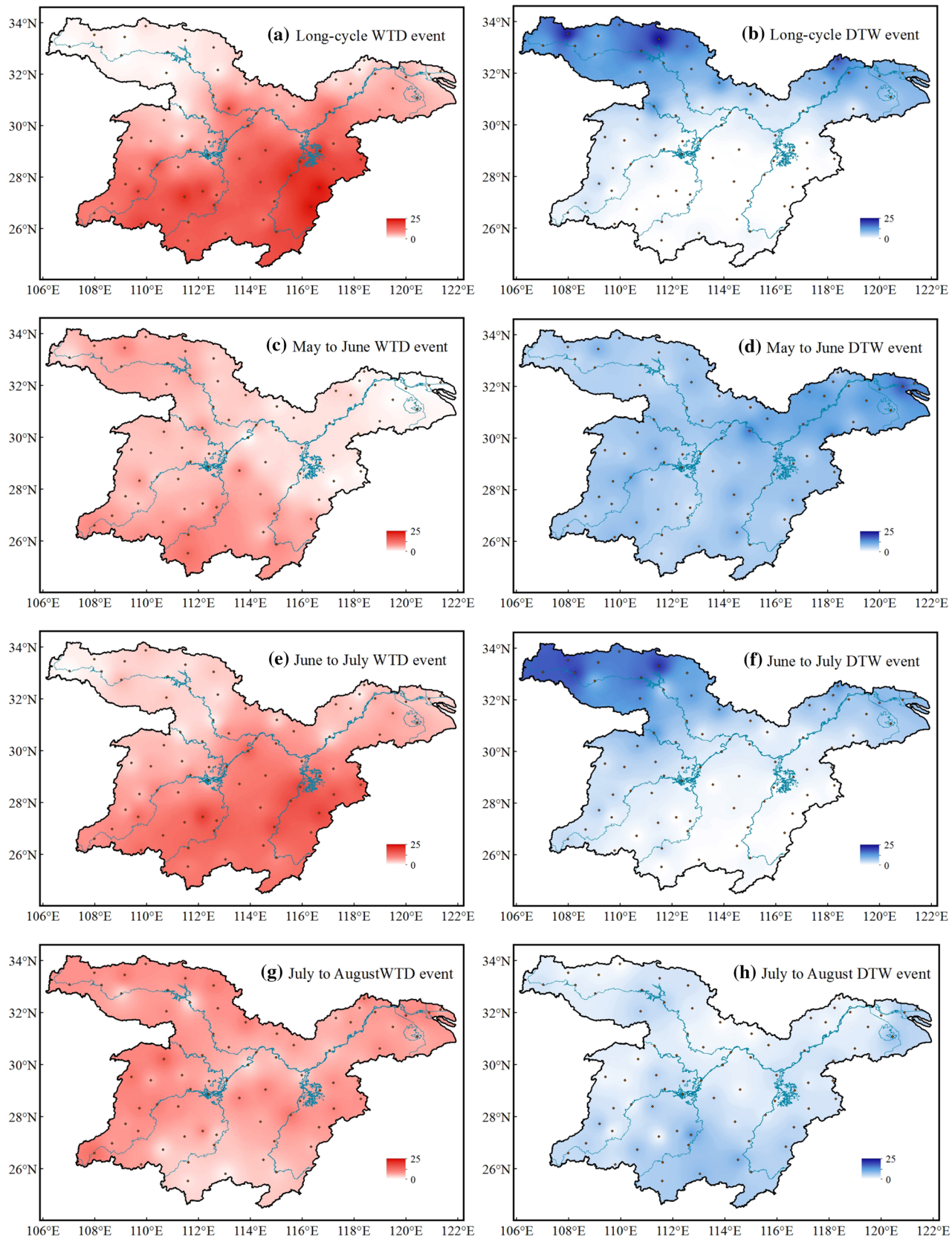

Fig. 3 Spatial distributions of the frequency of long-cycle (**a**, **b**) and short-cycle (**c**–**h**) DWAA events

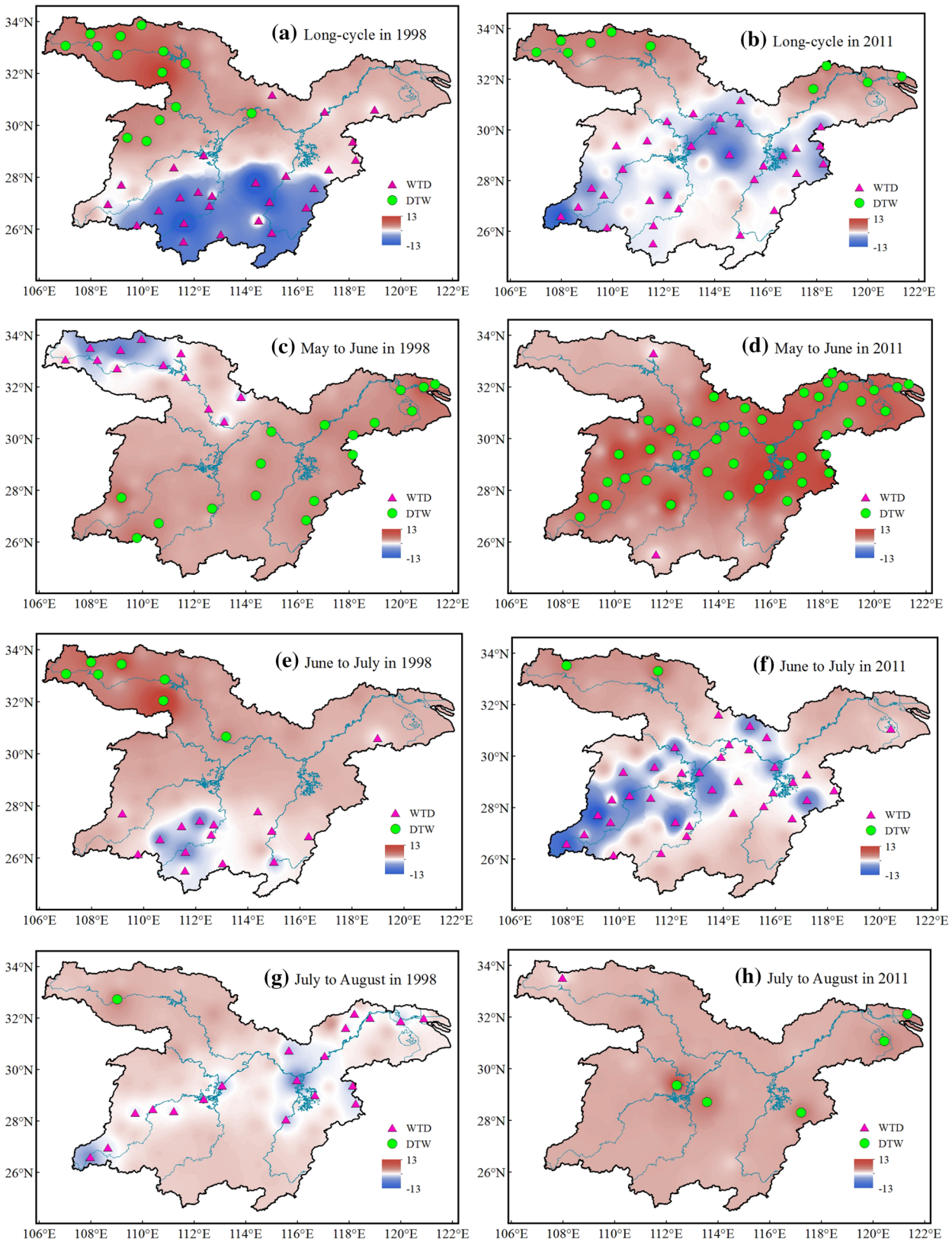

Fig. 4 Spatial distributions of the intensity of long-cycle (**a**, **b**) and short-cycle (**c**–**h**) DWAA events in 1998 and 2011. *Green circular* and *red triangles* represent the stations with DTW events and WTD events, respectively

noted that the long-cycle WTD events are very likely transforming into DTW events, especially in the Dongting Lake watershed. SDWAAI, which has predominantly positive values during the period of May–June (Fig. 5b), shows an increasing trend in the basin, except at Wuhan and Huangshi stations. Thus, the intensity of DTW events is declining at Wuhan and Huangshi stations, but increasing throughout the remainder of the basin. Similarly, the intensity of WTD events during the period of June–July has increased in the northwestern area (Fig. 5c), but has decreased throughout the remainder of the basin. As observed for the long-cycle DWAA events, short-cycle WTD events are also transforming into DTW events, especially in the Dongting Lake watershed. For the period of July–August (Fig. 5d), the intensity of WTD events is declining in the northwest and southeast regions, but increasing in the southwest, even showing a significant increase in the Dongting Lake watershed.

3.3 Early warning analysis of DWAA events

For LDWAA events, the selected predictive factors are listed in Table 3. A positive correlation exists between LDWAAI and North Africa subtropical high ridge line in September of the previous year, and negative correlations exist between LDWAAI and the following five indices: NAOI in May of the previous year; index of the strength of the polar vortex in Asia in May of the previous year; the ridge line of the Indian subtropical high in January of the current year; index of the northern extent of the Indian subtropical high in January of the current year, and index of the strength of the polar vortex in the Northern Hemisphere in February of the current year.

The DWAAI time series were ranked in the order of their values, and circulation indices of the corresponding years were then rearranged. The rearranged sequences can be classified into three types: DTW, WTD and normal conditions. The DTW and WTD classed include the 6 years with the highest and lowest DWAAI values, respectively, and the remaining 41 years correspond to normal conditions. First, the average values of the circulation indices of the three classes were calculated individually, and the variation trends of the predictive factors with increasing DWAAI values were then analyzed based on the correlation coefficients test. Based on the above method, the early warning signals that portend DWAA events could be identified. For the LDWAA events, the trends and relationships between the LDWAAI

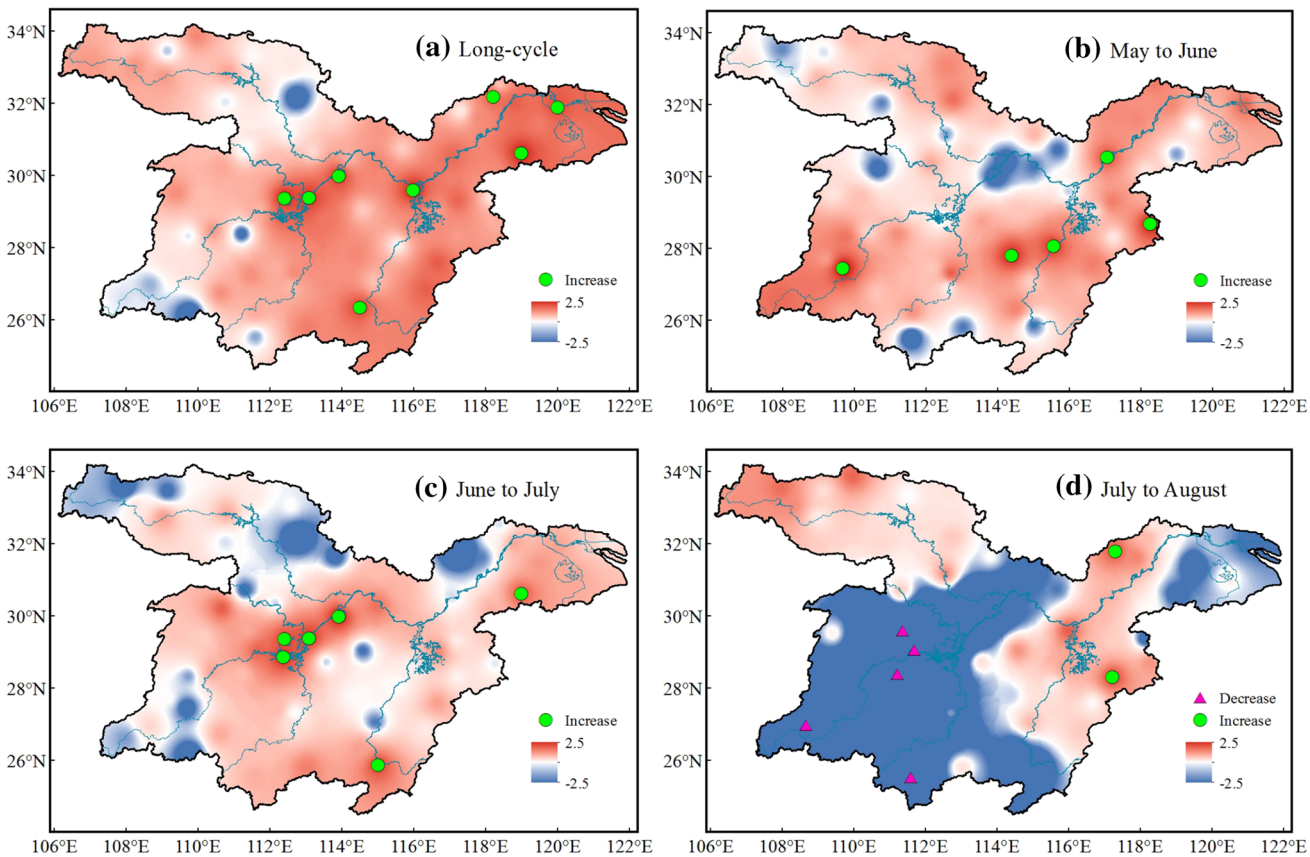

Fig. 5 Spatial distributions of the trends of variation in long-cycle (**a**) and short-cycle (**b**–**d**) DWAA events. Stations with significant increasing and decreasing trends are shown as *green circular* and *red triangles*

Table 3 Tendencies of the predictive factors of long -cycle DWAA events

Predictive factor	Month	Event type			Tendency	Correlation coefficient
		WTD	Normal	DTW		
The ridge line of the Indian subtropical high (65E–95E)	January of the current year	11.83	10.39	10.67	–	–
The ridge line of the North African subtropical high (20W–60E)	September of the previous year	21.83	23.32	22.83	–	–
Index of the northern extent of the Indian subtropical high (65E–95E)	January of the current year	13.00	10.88	11.83	–	–
Index of the strength of the polar vortex in Asia (region 1, 60E–150E)	May of the previous year	45.17	40.98	42.83	–	–
NAOI	May of the previous year	0.73	−0.22	−0.39	↓	−0.152
Index of the strength of the polar vortex in the Northern Hemisphere (region 5, 0–360)	February of the current year	360.17	349.95	345.33	↓	**−0.301**

Boldface indicating the tendencies of their corresponding series surpass the 0.05 significance level

and the predictive factors are shown in Fig. 6 and Table 3.

Different circulation patterns have different influences on DWAA events. Only two predictive factors that exhibit decreasing trends with an increasing LDWAAI, i.e., NAOI in May of the previous year and the index of the strength of the polar vortex in the Northern Hemisphere in February of the current year. Notably, the correlation coefficient between the index of the strength of the polar vortex in the Northern Hemisphere in February of the current year and the increasing LDWAAI series is as high as −0.301, which surpasses the 0.05 significance level. Therefore, years in which the index in February of the current year is greater than 360.17 have a high probability of the occurrence of long-cycle WTD events. However, long-cycle DTW events are still possible when the index is less than 345.33. Therefore, the index of the strength of the polar vortex in the Northern Hemisphere in February of the current year can be a suitable early warning signal for the occurrence of long-cycle DWAA events. The critical values of the early warning signals identified based on the analysis approach described above are listed in Table 4.

3.4 Simulation and prediction

The DWAAI series from 1960 to 2012 were divided into a calibration period (1960–1997) and a validation period (1998–2012). The index of qualified rate was used to evaluate the prediction accuracy. A qualified event is defined as a scenario in which the event type determined by the simulation is identical to the real observation from the same year.

The prediction accuracy results corresponding to DWAA events with different cycles simulated using the BP neural network model are shown in Table 5. During the calibration period, the performance values of the BP neural network method for DWAA events are above 81%, and the average is nearly 14% higher than that in the verification period. Comparison of the simulation accuracy of the model for both LDWAA and SDWAA events shows that the results for all SDWAA events are superior to those for LDWAA events, for both calibration and verification period, except in the case of the verification period of the DWAA events during the period of May–June, as the qualified rate value of 60.00% is slightly lower than that of 66.67% for the long-cycle DWAA events. Moreover, the qualified rates of the method for periods of June–July and July–August are all up to 80%, which are 20% higher than that in the period of May–June.

Comparisons of the actual and simulated DWAAI by BP neural network are shown in Fig. 7. In calibration period, the simulated DWAAI values, even the outliers, are in almost perfect agreement with the actual results. Moreover, the general trends of the predicted values, in the verification period also approximately agree with those of the different cycles. These results reveal that the BP neural network method is an efficient tool for simulating the occurrence of DWAA events.

4 Conclusions

The spatial and temporal characteristics of the intraseasonal DWAA events over YRB-ML were analyzed by calculating the DWAAI values. Correlation coefficients and a stepwise regression model were applied to select potential predictive factors, and suitable early warning signals were then identified based on the correlation

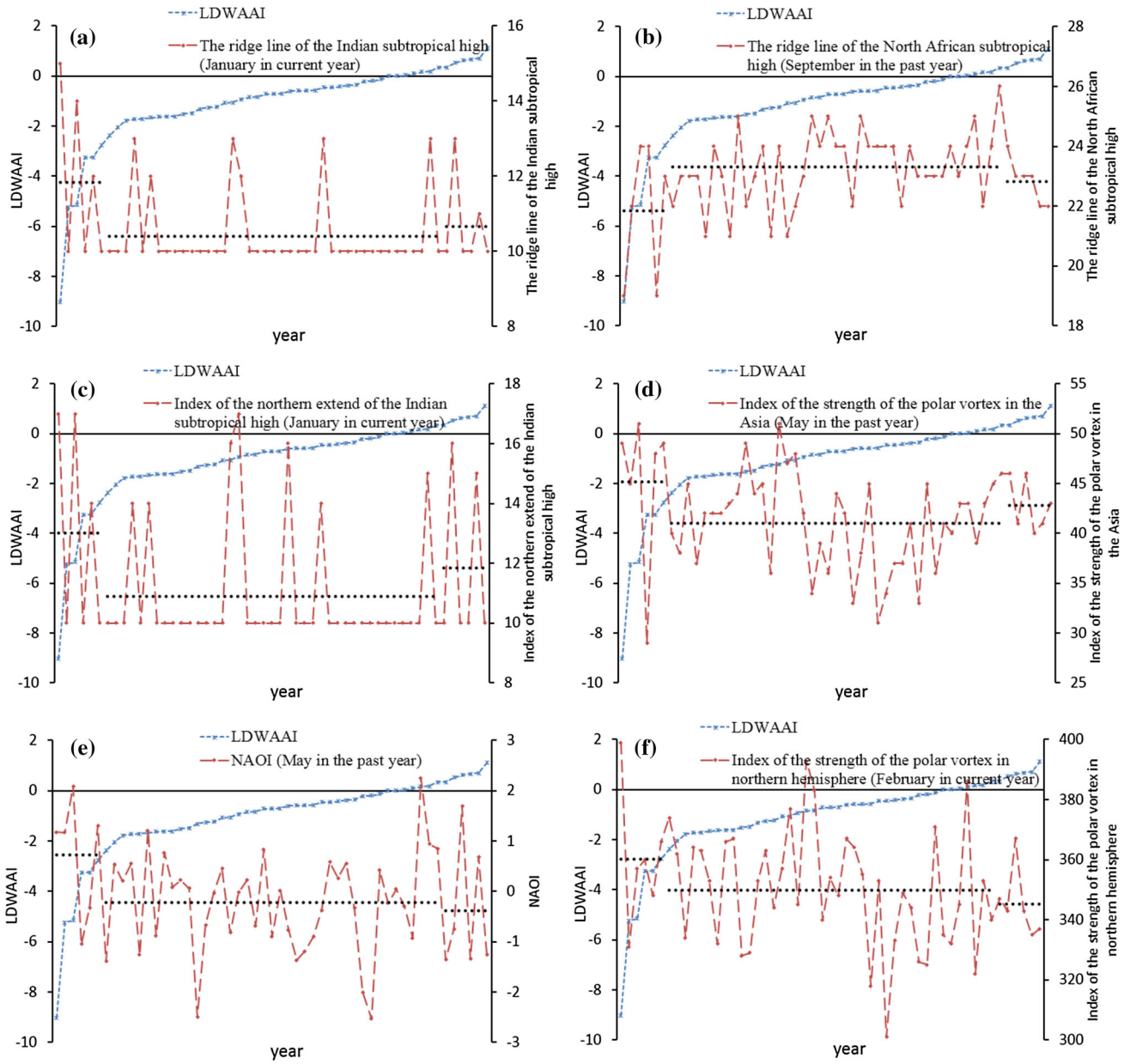

Fig. 6 Trends and relationships between the LDWAAI and its six predictive factors. *Blue* and *red lines* (*dots*) represent LDWAAI values listed by ascending counts and circulation indices of the corresponding years, respectively. *Black dotted lines* represent the average values of circulation indices in the three classes (from *left* to *right*: WTD, normal conditions and DTW)

coefficients test. Subsequently, a BP neural network model was applied to simulate DWAA events. The results are summarized as follows:

1. The temporal evolution characteristics of DWAA events were evaluated in terms of the entire basin. The main type of LDWAA and SDWAA events during the periods of June–July and July–August was WTD, and the frequency and intensity have gradually decreased over time. However, DTW was the main type of SDWAA events during the period of May–June, and the frequency and intensity increased over time.
2. The spatial distribution characteristics were analyzed in terms of three aspects: frequency, intensity and trends. High-intensity and high-frequency long-cycle DTW events and DTW events during the period of June–July were concentrated in the northwestern part of the basin, and no significant increasing or decreasing trends were observed. While WTD events of the same time scale were centered in the southeastern part and the middle reaches of the river, and a significant decreasing trend was present in the Dongting Lake

Table 4 Tendencies and critical values of the early warning signals of DWAA events

Period	Predictive factor	Month	Event type			Tendency	Correlation coefficient	Significance
			WTD	Normal	DTW			
Long-cycle	NAOI	May of the previous year	0.73	−0.22	−0.39	↓	−0.152	No
	Index of the strength of the polar vortex in the Northern Hemisphere (region 5, 0–360)	February of the current year	360.17	349.95	345.33	↓	**−0.301**	**Yes**
May–June	Index of the northern extent of the North American subtropical high (110W–60W)	December of the previous year	17.67	18.95	20.33	↑	0.269	No
	Index of the northern extent of the Northern Hemisphere subtropical high (5E–360)	November of the previous year	22.00	21.44	20.67	↓	−0.210	No
	Index of the strength of the polar vortex in the Northern Hemisphere (region 5, 0–360)	May of the previous year	160.50	158.80	143.50	↓	−0.249	No
June–July	Index of the northern extent of the subtropical high over the western Pacific (110E–150E)	June of the previous year	27.00	26.05	24.33	↓	**−0.340**	**Yes**
	Index of the area of the North African subtropical high (20W–60E)	October of the previous year	14.33	20.29	23.50	↑	**0.279**	**Yes**
	NAOI	September of the previous year	0.48	−0.21	−0.56	↓	−0.097	No
	Index of the strength of the polar vortex in North America (region 3, 120W–30W)	February of the current year	110.50	97.37	87.83	↓	**−0.523**	**Yes**
July–August	Index of the area of the polar vortex in the Atlantic and European sector (region 4, 30W–60E)	March of the current year	158.00	169.49	182.33	↑	**0.330**	**Yes**
	Index of the strength of the center of the polar vortex in the Northern Hemisphere (JQ)	July of the previous year	36.50	42.17	42.17	↑	**0.280**	**Yes**

Boldface indicating the tendencies of their corresponding series surpass the 0.05 significance level

Table 5 BP neural network model simulation results for DWAA events

Period	Qualified rate (%)				
	Long-cycle	Short-cycle			
		May–June	June–July	July–August	Average
Calibration period	81.58	92.11	86.84	84.21	87.72
Verification period	66.67	60.00	80.00	80.00	73.33

watershed. Importantly, high-intensity and high-frequency DTW events with significant increasing trends in the period of May–June occurred in most parts of the basin. The frequency and intensity of DWAA events in the period of July–August were relatively small, and the spatial distributions were more uniform.

3. Early warning signals that exhibit significant trends of variation with an increasing DWAAI values could be used to help predict the occurrence of DWAA events by comparing actual values to the critical values of these warning parameters. DWAA events with different cycles have different early warning signals.
4. The BP neural network approach was beneficial for simulating DWAA events. For the simulations of SDWAA events, the average qualified rate during the verification period was as high as 73.33%, markedly

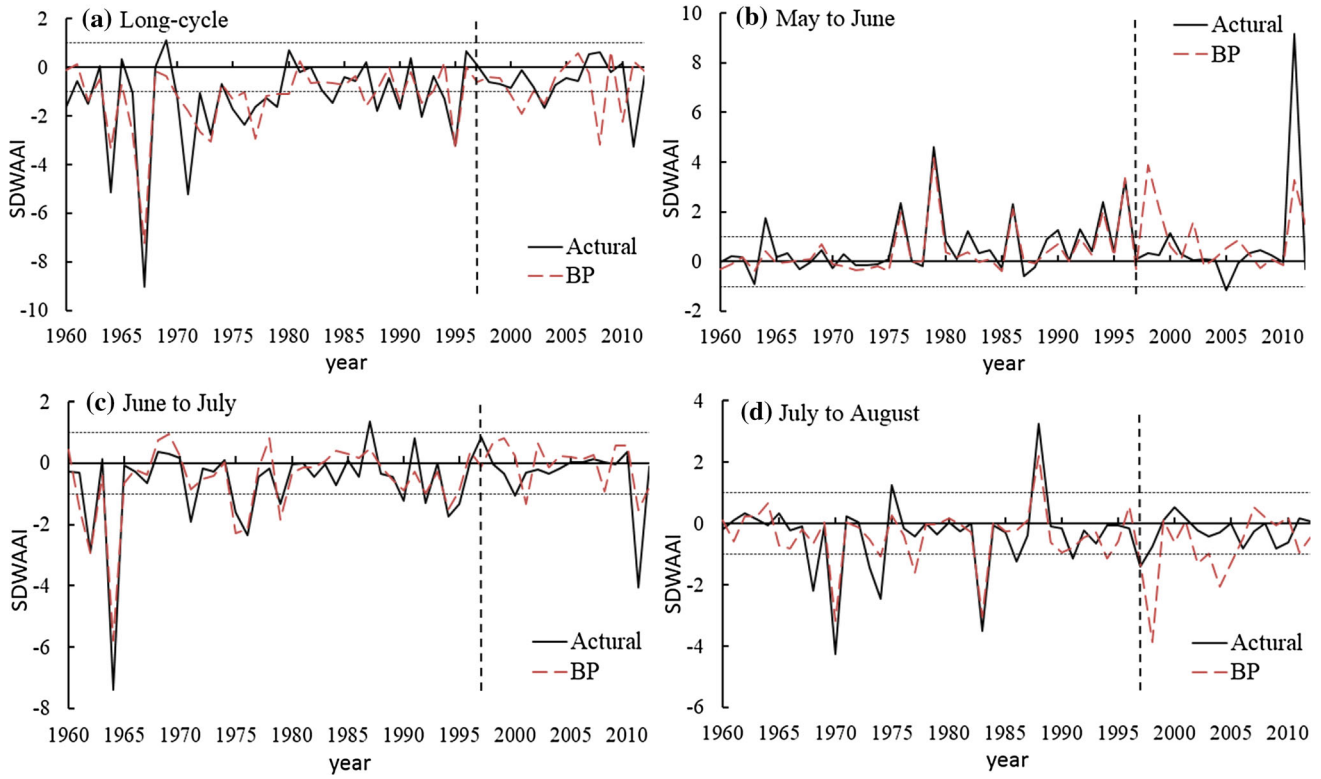

Fig. 7 Time series of **a** LDWAAI and SDWAAI during periods of **b** May–June, **c** June–July and **d** July–August of YRB-ML. *Red dashed lines* and *black solid lines* represent the simulated and actual DWAAI values, respectively

higher than that for LDWAA events. Therefore, this approach may serve as a useful reference for intraseasonal wet and dry management in the Yangtze River Basin.

Acknowledgements This study was supported by the State Key Program of National Natural Science of China (No. 51339004) and the National Natural Science Foundation of China (No. 51279139).

References

Bilgili M (2010) Prediction of soil temperature using regression and artificial neural network models. Meteorol Atmos Phys 110:59–70

Camberlin P (1997) Rainfall anomalies in the source region of the Nile and their connection with the Indian summer monsoon. J Clim 10:1380–1392

Cevik A (2007) Unified formulation for web crippling strength of cold-formed steel sheeting using stepwise regression. J Constr Steel Res 63:1305–1316

Chaudhuri S, Pal J (2014) The influence of El Nino on the Indian summer monsoon rainfall anomaly: a diagnostic study of the 1982/83 and 1997/98 events. Meteorol Atmos Phys 124:183–194

Cheng Z, Xu M, Luo LS, Ding XJ (2012) Climate characteristics of drought-flood abrupt change events in Huaihe River Basin. J China Hydrol 32:73–79

Chikoore H, Jury MR (2010) Intraseasonal variability of satellite-derived rainfall and vegetation over Southern Africa. Earth Interact 14:1–26

Efstathiou MN, Varotsos CA (2012) Intrinsic properties of Sahel precipitation anomalies and rainfall. Theor Appl Climatol 109:627–633

Fausett L (1994) Fundamentals of neural networks: Architectures, Algorithms, and Applications. Prentice Hall, Englewood Cliffs, NJ

French MN, Krajewski WF, Cuykendall RR (1992) Rainfall forecasting in space and time using a neural network. J Hydrol 137:1–31

Ghani IMM, Ahmad S (2010) Stepwise multiple regression method to forecast fish landing. Proc Soc Behav Sci 8:549–554

Ghorbani MA, Khatibi R, FazeliFard MH, Naghipour L, Makarynskyy O (2016) Short-term wind speed predictions with machine learning techniques. Meteorol Atmos Phys 128:57–72

Gonzalez PLM, Vera CS, Liebmann B, Kiladis G (2008) Intraseasonal variability in subtropical South America as depicted by precipitation data. Clim Dyn 30:727–744

Groisman PY, Karl TR, Easterling DR, Knight RW, Jamason PF, Hennessy KJ, Suppiah R, Page CM, Wibig J, Fortuniak K, Razuvaev V, Douglas A, Rorland E, Zhai PM (1999) Changes in the probability of heavy precipitation: important indicators of climatic change. Clim Change 42:243–283

Hammerstrom D (1993) Working with neural networks. IEEE Spectr 30:46–53

Haykin S (1994) Neural networks, a comprehensive foundation. Prentice-Hall Inc, Upper Saddle River

Ho CH, Lee JY, Ahn MH, Lee HS (2003) A sudden change in summer rainfall characteristics in Korea during the late 1970s. J Clim 23:117–128

Karunanithi N, Grenney WJ, Whitley D, Bovee K (1994) Neural networks for river flow prediction. J Comput Civ Eng 8:201–220

Kendall MG (1975) Rank correlation methods. Griffin, London

Kim D, Lee M-I, Kim D, Schubert SD, Waliser DE, Tian B (2014) Representation of tropical subseasonal variability of precipitation in global reanalyses. Clim Dyn 43:517–534

Kruger AC (1999) The influence of the decadal-scale variability of summer rainfall on the impact of El Nino and La Nina events in South Africa. Int J Clim 19:59–68

Li XH, Ye XC (2015) Spatiotemporal characteristics of dry–wet abrupt transition based on precipitation in Poyang Lake Basin, China. Water 7:1943–1958

Maheras P, Xoplaki E, Kutiel H (1999) Wet and dry monthly anomalies across the Mediterranean Basin and their relationship with circulation, 1860–1990. Theor Appl Climatol 64:189–199

Mann HB (1945) Nonparametric tests against trend. Econometrica 13:245–259

Muhire I, Ahmed F, Abutaleb K (2015) Relationships between Rwandan seasonal rainfall anomalies and ENSO events. Theor Appl Climatol 122:271–284

Reason CJC, Hachigonta S, Phaladi RF (2005) Interannual variability in rainy season characteristics over the Limpopo region of southern Africa. Int J Clim 25:1835–1853

Rumelhart DE, Hinton GE, Williams RJ (1986) Learning representations by back-propagating errors. Nature 323:533–536

Schaer C, Frei C, Luthi C, Davies HC (1996) Surrogate climate change scenarios for regional climate models. Geophys Res Lett 23:669–672

Shamseldin AY (1997) Application of a neural network technique to rainfall-runoff modelling. J Hydrol 199:272–294

Shen BZ, Zhang SX, Yang HW, Wang K, Feng GL (2012) Analysis of characteristics of a sharp turn from drought to flood in the middle and lower reaches of the Yangtze River in spring and summer in 2011. Acta Phys Sin 61:1–11

Su BD, Jiang T, Jin WB (2006) Recent trends in observed temperature and precipitation extremes in the Yangtze River basin, China. Theor Appl Climatol 83:139–151

Sun P, Liu CL, Zhang Q (2012) Spatio-temporal variations of drought-flood abrupt alternation during main flood season in East River Basin. Pearl River 5:29–34

Tao SY, Ding YH (1981) Observational evidence of the influence of the Qinghai-Xizang plateau on the occurrence of heavy rain and severe convective storms in China. Bull Am Meteorol Soc 62:23–30

Turner AG, Annamalai H (2012) Climate change and the South Asian summer monsoon. Nat Clim Change 2:587–595

Weaver SJ, Ruiz-Barradas A, Nigam S (2009) Pentad evolution of the 1988 drought and 1993 flood over the great plains: an NARR perspective on the atmospheric and terrestrial water balance. J Clim 22:5366–5384

Wu ZW, Li JP, He JH, Jiang ZH (2006) Large-scale atmospheric singularities and summer long-cycle droughts-floods abrupt alternation in the middle and lower reaches of the Yangtze River. Chin Sci Bull 51:2027–2034

Yao SX, Huang Q, Li T, Zhang CY (2014) The intraseasonal oscillations of precipitation and circulations from January to March in 2010 in East Asia. Meteorol Atmos Phys 123:67–79

Zhang Y, Wang WC (1997) Model-simulated northern winter cyclone and anticyclone activity under a greenhouse warming scenario. J Clim 10:1616–1634

Zhang XW, Xu WG, Shi HJ, Han CS (2007) Understanding and studies of law of sudden turn of drought and flood in Anhui Province. China Water Resour 5:40–42

Zhang SF, Zhang JC, Min JJ, Zhang ZX, Zhuang JY, Lin J (2012) Drought-flood abrupt alternation based on runoff in the Huaihe River Basin during rainy season. J Lake Sci 24:679–686